A Superconducting Maglev Vehicle/Guideway System With Preview Control: Part II—Controller Design and System Behavior

S. K. Wang
Spacecraft Bus Electronics,
Hughes Space and
Communications Company,
2000 E. El Segundo Boulevard,
El Segundo, CA 90245-4709

M. L. Nagurka
Department of Mechanical and
Industrial Engineering,
Marquette University,
Milwaukee, WI 53201-1881

Part II of this paper proposes the use of optimal preview control with integral action for a maglev vehicle with a superconducting electromagnetic suspension system operating on an elevated, flexible guideway. The control system is designed based on a linearized model and then applied to a full-scale nonlinear simulation model of the maglev vehicle, magnet modules, and guideway (derived in Part I—Vehicle, Guideway, and Magnet Modeling). Simulation studies demonstrate the effectiveness of the controller and evaluate the vehicle performance under the influences of guideway flexibility, guideway irregularities, and aerodynamic disturbances.

1 Introduction

A primary safety requirement for maglev dynamic performance is the ability to operate over a wide range of conditions without leaving or contacting the guideway. In maglev systems that rely on electromagnetic suspension (EMS) forces, this requirement is accomplished via active feedback control (Heinrich and Kretzschmar, 1989). The control system plays multiple roles, one of which is to ensure overall safe performance by actively positioning the vehicle relative to the guideway to maintain a nominal levitation air gap. The controller also tunes the suspension impedance to attain acceptable ride quality.

Conventional linear quadratic (LQ) optimal control has been utilized to stabilize an EMS maglev system and regulate the air gap (Kortüm and Utzt, 1984). However, a nonzero steady-state gap error can result due to constant disturbances, such as a step guideway offset or a constant aerodynamic load. To circumvent this problem, an optimal integral control technique (Anderson and Moore, 1990) can be applied in which integrators are inserted in the controller to eliminate steady-state errors due to constant disturbances. Furthermore, if information about the disturbance input is known a priori, it can be used by an extended LQ optimal controller, called an optimal preview controller (Bender, 1968; Tomizuka, 1976), to improve performance of the suspension. With the advent of modern microcomputer technology, optimal preview control has become a practical option. It has been proposed for automotive applications (Hać, 1992; Louam et al., 1992; Peng and Tomizuka, 1993; Langlois and Anderson, 1995) and train applications (Jezequel and Roberti, 1996; Fujioka and Yamada, 1996), but it has not been studied in maglev vehicle designs.

In Part II of this paper a LQ optimal control strategy with integral action and preview is proposed. As noted, the integral action ensures zero steady-state gap error due to step disturbances. The preview controller, using guideway information (obtained from a sensor looking ahead of the vehicle or from a database of guideway irregularities obtained independently), promises to improve the vehicle dynamic performance. To test its effectiveness, the preview controller is combined with the detailed maglev/guideway model developed in Part I to form a complete nonlinear simulation model. Simulation results of this comprehensive model under the influence of guideway flexibility, guideway irregularities, and cross-wind gust are reported, where performance is measured in terms of gap error for safety, vehicle vertical and lateral accelerations for ride comfort, and magnet input voltage for energy cost.

Contributed by the Dynamic Systems and Control Division for publication in the JOURNAL OF DYNAMIC SYSTEMS, MEASUREMENT, AND CONTROL. Manuscript received by the DSCD December 19, 1995. Associate Technical Editor: G. Rizzoni.

2 Preview Control Scheme

The proposed control method requires a linearized plant model to design the control law. In Section 2.1, a linear model for the maglev vehicle with superconducting (SC) magnet modules is first introduced. Based on this model, an optimal preview control law is presented in Section 2.2.

2.1 Plant Linearization. The nonlinear plant model derived in Part I of this paper is linearized about the nominal point where all plant state variables are set to zero and the air gap at each magnet module is equal to the nominal air gap, h_0. Detailed derivations are given by Wang (1995).

The linearized plant model can be represented by the state and output equations

$$\dot{\mathbf{x}}_p = \mathbf{A}_p\mathbf{x}_p + \mathbf{B}_p\mathbf{u} + \mathbf{E}_p\mathbf{v}, \quad \mathbf{y} = \mathbf{C}_p\mathbf{x}_p + \mathbf{D}_p\mathbf{v} \quad (1), (2)$$

where the state vector, $\mathbf{x}_p$, disturbance vector, $\mathbf{v}$, control vector, $\mathbf{u}$, and output vector, $\mathbf{y}$, can be identified as

$$\mathbf{x}_p = \begin{bmatrix} \mathbf{x}_v \\ \mathbf{i} \end{bmatrix} = [y_c, z_c, \phi_c, \theta_c, \psi_c, \omega_x, \omega_y, \omega_z, i_1, \ldots, i_{2N_m}]^T \quad (3)$$

$$\mathbf{v} = [y_{g1}, \ldots, y_{g(2N_m)}, z_{g1}, \ldots, z_{g(2N_m)}, \dot{y}_{g1}, \ldots, \dot{y}_{g(2N_m)}, \dot{z}_{g1}, \ldots, \dot{z}_{g(2N_m)}, F_w, M_w]^T \quad (4)$$

$$\mathbf{u} = [u_1, \ldots, u_{2N_m}]^T, \quad (5)$$

$$\mathbf{y} = [h_1 - h_0, \ldots, h_{2N_m} - h_0]^T \quad (6)$$

and where the coefficient matrices are $\mathbf{A}_p$, $\mathbf{B}_p$, $\mathbf{C}_p$, $\mathbf{D}_p$, and $\mathbf{E}_p$. Equations (1) and (2) represent the linear plant which is a $(10 + 2N_m)$-th order system with $2N_m$ control inputs, $2N_m$ outputs,

and $2 + 8N_m$ disturbances. With the linear plant model, the behavior of the open-loop system (i.e., maglev vehicle with SC magnets but without controller) can be examined through the eigenvalues of the system matrix, $\mathbf{A}_p$, and the control law can be derived based on the linearized state and output equations.

2.2 Optimal Preview Control With Integral Action. In order to eliminate nonzero steady-state gap errors due to constant disturbances, the linear plant is augmented by adding integrators at its outputs. The integrator dynamics are then

$$\mathbf{y} = \dot{\mathbf{y}}_I = \mathbf{C}_p\mathbf{x}_p + \mathbf{D}_p\mathbf{v} \tag{7}$$

where $\mathbf{y}_I$ is the integrator state vector. The augmented system dynamics are represented by the combination of the plant dynamics (1)–(2) and the integrator dynamics (7), and can be written as

$$\dot{\mathbf{x}} = \mathbf{A}\mathbf{x} + \mathbf{B}\mathbf{u} + \mathbf{E}\mathbf{v}, \quad \mathbf{y} = \mathbf{C}\mathbf{x} + \mathbf{D}\mathbf{v} \quad (8), (9)$$

where

$$\mathbf{A} = \begin{bmatrix} \mathbf{A}_p & \mathbf{O} \\ \mathbf{C}_p & \mathbf{O} \end{bmatrix}, \quad \mathbf{B} = \begin{bmatrix} \mathbf{B}_p \\ \mathbf{O} \end{bmatrix}, \quad \mathbf{C} = [\mathbf{C}_p \quad \mathbf{O}], \quad (10)-(12)$$

$$\mathbf{D} = \mathbf{D}_p, \quad \mathbf{E} = \begin{bmatrix} \mathbf{E}_p \\ \mathbf{D}_p \end{bmatrix}, \quad \mathbf{x} = \begin{bmatrix} \mathbf{x}_p \\ \mathbf{y}_I \end{bmatrix} \quad (13)-(15)$$

The proposed control system applies LQ optimal preview control to the augmented system. The resulting control law can be expressed as (Hać, 1992)

$$\mathbf{u}(t) = -\mathbf{K}_c\mathbf{x}(t) - \mathbf{R}^{-1}\mathbf{B}^T\mathbf{r}(t) \tag{16}$$

where

$$\mathbf{K}_c = \mathbf{R}^{-1}\mathbf{B}^T\mathbf{P}, \tag{17}$$

$$\mathbf{P}\mathbf{A} + \mathbf{A}^T\mathbf{P} - \mathbf{P}\mathbf{B}\mathbf{R}^{-1}\mathbf{B}^T\mathbf{P} + \mathbf{Q} = \mathbf{O} \tag{18}$$

$$\mathbf{r}(t) = \int_0^{t_p} e^{(\mathbf{A}-\mathbf{B}\mathbf{R}^{-1}\mathbf{B}^T\mathbf{P})^T\sigma}\mathbf{P}\mathbf{E}\mathbf{v}(t+\sigma)d\sigma \tag{19}$$

where t_p is the preview time and $\mathbf{Q}$ and $\mathbf{R}$ are symmetric weighting matrices which are semi-positive and positive definite, respectively. From optimal control theory, it can be shown that the optimal control, $\mathbf{u}(t)$, exists and the resulting closed-loop system is asymptotically stable if the system $(\mathbf{A}, \mathbf{B})$ is stabilizable and the system $(\mathbf{A}, \mathbf{H})$, where $\mathbf{H}$ is a square matrix with $\mathbf{H}^T\mathbf{H} = \mathbf{Q}$, is detectable (Hać, 1992).

Table 1 Parameters of maglev model

Parameter	Symbol	Value	Unit
vehicle mass	M_v	30,600	kg
vehicle length	L_v	18	m
vehicle height	h_v	3.9	m
vehicle width	w_v	3.8	m
nominal air gap	h_0	0.04	m
height, magnet centroid to vehicle CG	h_c	1.09	m
width, magnet centroid to vehicle CG	w_c	0.76	m
roll moment of inertia	I_x	7.4×10^4	kg-m^2
pitch moment of inertia	I_y	8.0×10^5	kg-m^2
yaw moment of inertia	I_z	9.6×10^5	kg-m^2
magnet cant angle	β	35	deg
number of modules on each side	N_m	2	None
number of magnets in each module	n_m	12	None
number of turns in SC coil	N_{SC}	1020	None
number of turns in normal coils	N_n	96	None
face area of each magnetic pole	A_m	0.04	m
total resistance of normal coils	R_c	1.0	ohm
permeability of air	μ_0	$4\pi\times10^{-7}$	weber/A-m
span length	L_s	21.3	m
span mass per unit length	γ	4777	kg-m^2
bending rigidity	EI	1.84×10^{10}	N-m^2
first-mode span damping ratio	ζ	0.03	None

Table 2 Eigenvalues of open-loop system

Symbol	Eigenvalue	Damping Ratio	Natural Freq. (rad/s)
$\lambda_{o,1}$ & $\lambda_{o,2}$	$-0.158 \pm j18.5$	0.00851	18.5
$\lambda_{o,3}$ & $\lambda_{o,4}$	$-0.370 \pm j1.49$	0.241	1.5
$\lambda_{o,5}$	−11.7	1.0	11.7
$\lambda_{o,6}$	−16.4	1.0	16.4
$\lambda_{o,7}$	−18.8	1.0	18.8
$\lambda_{o,8}$	16.4	−1.0	16.4
$\lambda_{o,9}$	14.5	−1.0	14.5
$\lambda_{o,10}$	10.9	−1.0	10.9
$\lambda_{o,11}$	−170.3	1.0	170.3
$\lambda_{o,12}$	−170.9	1.0	170.9
$\lambda_{o,13}$	−171.6	1.0	171.6
$\lambda_{o,14}$	−172.0	1.0	172.0

The control law (16) consists of a feedback part (first term) and a feedforward part (second term). The optimal feedback gain matrix, $\mathbf{K}_c$, in the feedback part is the same as the one used in linear quadratic regulator (LQR) problems. Consequently, many linear quadratic (LQ) design methods developed in the literature can be applied to select the appropriate weighting matrices and shape the required system response. The input to the feedforward part is the preview information, $\mathbf{v}(t + \sigma)$ for $\sigma \in [0, t_p]$. If no preview information is available, the controller consists solely of the feedback controller.

2.3 Control System Design. The weighting matrices $\mathbf{Q}$ and $\mathbf{R}$ are two controller design parameters chosen to meet the required performance specifications, such as appropriate bandwidth and relative stability, and limits on key state and control variables. In this work, a conventional method of selecting $\mathbf{Q}$ and $\mathbf{R}$ suggested by Bryson and Ho (1969) is adopted:

$$\mathbf{Q} = \text{diag}\,(y_{\max}^{-2}, z_{\max}^{-2}, \phi_{\max}^{-2}, \theta_{\max}^{-2}, \psi_{\max}^{-2}, \dot{y}_{\max}^{-2}, \dot{z}_{\max}^{-2}, \omega_{x,\max}^{-2}, \omega_{y,\max}^{-2}, \omega_{z,\max}^{-2}, i_{1,\max}^{-2}, \ldots, i_{2N_m,\max}^{-2}, y_{I1,\max}^{-2}, \ldots, y_{I(2N_m),\max}^{-2}) \tag{20}$$

$$\mathbf{R} = \text{diag}\,(u_{1,\max}^{-2}, \ldots, u_{2N_m,\max}^{-2}) \tag{21}$$

The limit on the lateral and vertical CG displacements is selected as $y_{\max} = z_{\max} = 0.01$ m which is of the same order of magnitude as the allowed gap variation. The limit on the roll, pitch, and yaw displacements is chosen as a low $\phi_{\max} = \theta_{\max} = \psi_{\max} = 0.01$ rad (0.57°) to reflect the physical constraints on these displacements. A maximum current of 300 A is used for the estimated limit of the trim currents, $i_{j,\max}(j = 1, \ldots, 2N_m)$. Since a unity D.C. gain is desired for the magnet system, the limit on the voltages, $u_{j,\max}$ $(j = 1, \ldots, 2N_m)$, is chosen as 300 V. The weightings on the CG velocities affect the speed of vehicle response. They can be adjusted to achieve desired damping ratios and natural frequencies. These weightings are initially selected as $\dot{y}_{\max} = \dot{z}_{\max} = 1$ m/s and $\omega_{x,\max} = \omega_{y,\max} = \omega_{z,\max} = 1$ rad/s. The speed of integral action is dominated by the weightings on the integrator state variables where an estimated limit of $y_{Ij,\max} = 0.001$ m/s $(j = 1, \ldots, 2N_m)$ is initially selected. It should be noted that the translation of specifications into the selection of $\mathbf{Q}$ and $\mathbf{R}$ matrices is not straightforward nor unique, and often adjustments are needed. The controller is designed in an iterative process.

The properties of the open-loop system can be examined by calculating the eigenvalues of the linearized plant model. Using the maglev system parameters listed in Table 1, the eigenvalues and the corresponding damping ratios and natural frequencies can be determined. As summarized in Table 2, the first ten eigenvalues characterize the carbody motion without feedback control. The remaining eigenvalues are the inverses of the magnet time constants. The fact that the natural frequencies of the

Table 3 Eigenvalues of closed-loop system

Symbol	Eigenvalue	Damping Ratio	Natural Freq. (rad/s)
$\lambda_{c,1}$ & $\lambda_{c,2}$	$-4.31 \pm j16.6$	0.250	17.2
$\lambda_{c,3}$ & $\lambda_{c,4}$	$-7.65 \pm j13.0$	0.508	15.1
$\lambda_{c,5}$ & $\lambda_{c,6}$	$-12.2 \pm j13.9$	0.659	18.5
$\lambda_{c,7}$ & $\lambda_{c,8}$	$-13.1 \pm j13.3$	0.701	18.7
$\lambda_{c,9}$ & $\lambda_{c,10}$	$-20.3 \pm j15.0$	0.804	25.2
$\lambda_{c,11}$	-10.7	1.0	10.7
$\lambda_{c,12}$	-14.4	1.0	14.4
$\lambda_{c,13}$	-16.6	1.0	16.6
$\lambda_{c,14}$	-23.8	1.0	23.8
$\lambda_{c,15}$	-242.5	1.0	242.5
$\lambda_{c,16}$	-242.9	1.0	242.9
$\lambda_{c,17}$	-243.4	1.0	243.4
$\lambda_{c,18}$	-243.7	1.0	243.7

magnet eigenvalues ($\lambda_{o,11}, \ldots, \lambda_{o,14}$) are much larger than the natural frequencies of the carbody eigenvalues ($\lambda_{o,1}, \ldots, \lambda_{o,10}$) indicates a faster dynamic response for the magnets than for the carbody. The three eigenvalues located in the right half-plane indicate that the open-loop system is unstable.

The closed-loop system can be obtained by applying the feedback control law (16) to the augmented state Eq. (8). The eigenvalues of the closed-loop system matrix and the corresponding damping ratios and natural frequencies are summarized in Table 3. The first ten eigenvalues are the vehicle modes which are all located in the left half-plane. The unstable modes in the open-loop system have been shifted into the stable region. Also, the damping ratios of the very lightly damped modes, $\lambda_{o,1}$ and $\lambda_{o,2}$, are increased from 0.00851 to an acceptable value of 0.25 ($\lambda_{c,1}$ and $\lambda_{c,2}$), with the natural frequency almost unchanged. Other carbody modes are well damped with damping ratios greater than 0.5. For efficient use of the control effort, the carbody modes have been placed at approximately uniform distances from the origin, ranging from 15.1 to 25.2 rad/s. The integral action inserts four additional eigenvalues in the closed-loop system, represented by the eigenvalues from $\lambda_{c,11}$ through $\lambda_{c,14}$. The last four eigenvalues in Table 3 are the SC magnet modes which have larger natural frequencies, compared to the uncontrolled situation, implying faster magnet dynamics.

3 Maglev System Performance

3.1 Simulation Model. The complete nonlinear maglev system, consisting of the vehicle model, guideway model, SC magnet system, and controller, is represented by the block diagram of Fig. 1. The inputs to the overall system are the aerodynamic force and moment, F_w and M_w, due to the cross-wind gust, and the irregularity, $\mathbf{w}_d$, due to the guideway. If preview control is implemented, then there is an additional input, $\mathbf{v}$, representing the preview information in front of the vehicle. The outputs of the system are the air gap, $\mathbf{h}$, and the vehicle state, $\mathbf{x}_v$.

A cross-wind gust model presented by Garg and Barrows (1981) is used to compute the aerodynamic lateral force, F_w, and yaw moment, M_w, acting on the vehicle resulting from

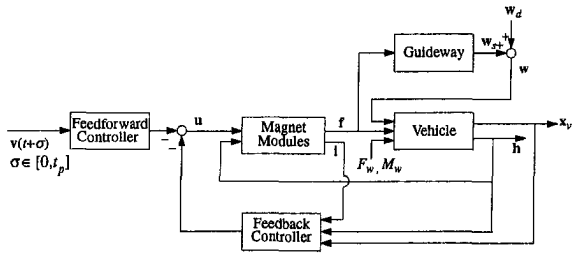

Fig. 1 Block diagram of complete maglev system

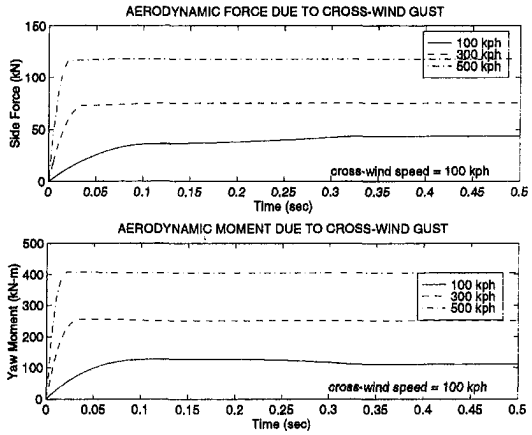

Fig. 2 Aerodynamic force and moment due to cross-wind gust

constant speed wind gusts. The cross-wind gust is assumed to be a wind profile perpendicular to the guideway with constant velocity. As the vehicle enters the wind zone, the vehicle responds to a sharp discontinuity, such as might occur when the vehicle exits a tunnel. This "knife-edge" wind gust model is a worst case. Figure 2 depicts the profiles of the aerodynamic lateral force and yaw moment for a 100 kph cross-wind gust at several vehicle speeds. The effects of the aerodynamic loading can be significant at high vehicle speed and may become a critical factor in control system design.

Guideway irregularities occur as a result of construction tolerances and environmental conditions. In this work, the guideway irregularity profile described in Snyder and Wormley (1977) is adopted which can be represented as the summation of the following effects: (*i*) surface roughness of the guideway iron rails, (*ii*) span vertical offsets due to misalignments of the guideway spans, (*iii*) column height variations, and (*iv*) intentionally imposed camber of the guideway spans to compensate for vehicle loading. Since these irregularities result from a wide variety of effects, it is assumed that the amplitudes of each type of irregularity (except for the surface roughness) are normally distributed random numbers. With prescribed mean values and standard deviations, the guideway irregularities may represent the tolerance requirements of the guideway structure. Figure 3 shows a combined guideway irregularity in the lateral and vertical directions, where the guideway roughness is in the normal direction of the rail face while the guideway steps, ramps, and cambers are in the vertical direction. The surface roughness is modeled by the power spectral density function (PSD) of the form: $\Phi(\Omega) = A_r/\Omega^2$, where A_r is a roughness parameter (Katz

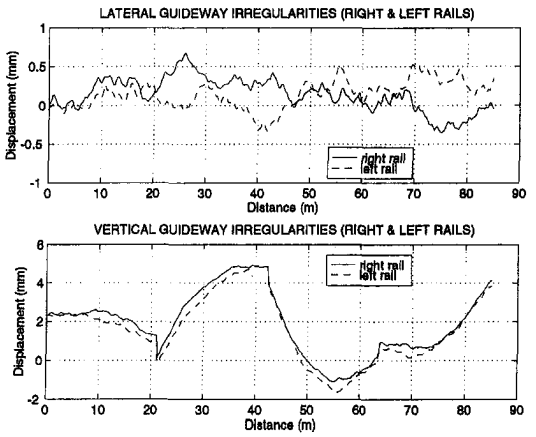

Fig. 3 Combined guideway irregularities

et al., 1974). Here, the guideway random roughness parameter, $A_r = 6.1 \times 10^{-8}$ m, representing a high quality welded rail (Wormley et al., 1992). The step deviation, column height, and camber amplitude for each span are generated randomly with a zero mean and a 2 mm standard deviation.

The dynamics of the complete maglev system are described by the combination of the dynamic equations of each subsystem: (*i*) ten first-order ordinary differential equations (ODEs) for the vehicle model, (*ii*) $2N_m$ first-order ODEs for the magnet modules, (*iii*) $2N_m$ first-order ODEs for the integrator dynamics in the feedback controller, and (*iv*) $2n_s$ second-order ODEs for the guideway flexibility for each of the two consecutive spans. The total number of state variables is $10 + 4(N_m + n_s)$. For a vehicle with four magnet modules (two per side) and a guideway modeled with three modes per span, thirty state variables are needed to characterize the complete system.

In the simulation model, it is assumed that the vehicle state, $\mathbf{x}_v$, the trim current, $\mathbf{i}$, and the air gap, $\mathbf{h}$, can be measured perfectly. Furthermore, when preview control is applied, it is assumed that the disturbance vector, $\mathbf{v}$, is available a priori.

3.2 Performance Studies. In the simulation studies, the maglev vehicle operates over a multi-span elevated guideway at constant speed. A number of safety-, energy- and comfort-related performance measures are posited for the maglev system. The maglev system is required to: (*i*) maintain each magnet module/iron rail air gap within a safe margin to prevent vehicle/guideway contact, (*ii*) ensure that the control voltages are within feasible limits, and (*iii*) attain maximum ride comfort.

The air gap is chosen to be 40 mm nominally with a ±10 mm maximum gap error. The smallest acceptable air gap of 30 mm precludes vehicle/guideway contact while assuring a reasonable safety margin. Gap deviation from the nominal value is viewed as a safety-related performance measure. The required control voltages are constrained within ±300 V to prevent saturation of the magnetic forces. The control voltage is used as an indication of energy cost. The ride comfort is measured by comparing carbody accelerations at the car front and rear to the ISO ride quality criteria (ISO, 1978). The ISO ride quality criteria specify limits on root mean square (RMS) lateral and vertical accelerations in one-third octave bands over a specified range of frequencies.

Both rigid and flexible guideways have been considered. Individual effects, such as cross-wind gusts and guideway flexibility, are investigated in Examples 1 and 2, respectively. Example 3 considers the overall performance of the maglev vehicle under the influences of guideway flexibility and combined guideway irregularities. In these examples, four magnet modules (two on each side) are assumed for the vehicle. In addition, the carbody roll, pitch, and yaw angles are assumed to be small. The assumption improves computational efficiency and is reasonable since the air gap is significantly smaller than the carbody dimensions. Finally, it is noted that the simulation results depend on the weighting matrices selected for the controller. A different control system optimization would alter the ride comfort, gap error and input voltage predictions and trade-offs.

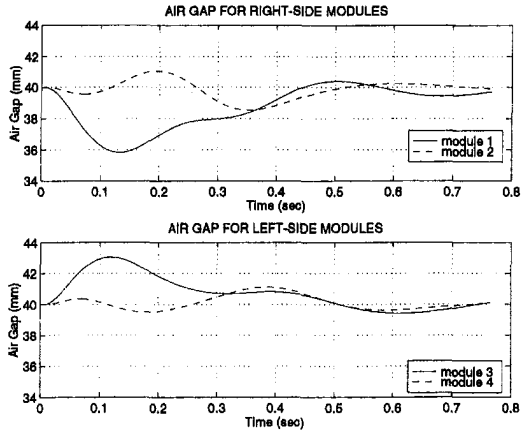

Fig. 4 Air gaps for case of cross-wind gust at 400 kph vehicle speed

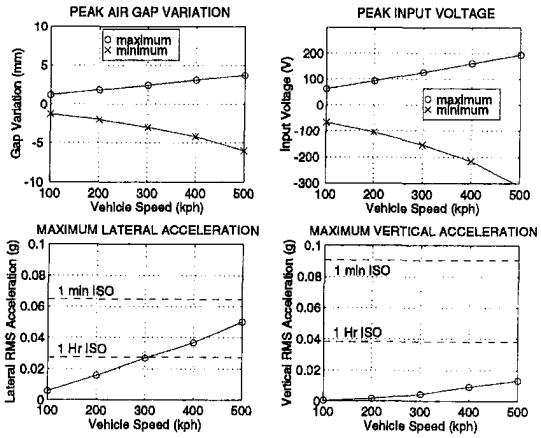

Fig. 5 Maglev system performance under a 100 kph cross-wind gust

3.2.1 Example 1: Vehicle Traversing a Cross-Wind Field. This example investigates the influence of cross-wind gust on the dynamic performance of the maglev vehicle. The vehicle is traveling on a rigid guideway subject to a strong cross-wind gust of 100 kph. The corresponding aerodynamic force and moment used in this example were shown previously in Fig. 2. It is assumed that preview information is not provided. Simulation studies were performed at five different vehicle speeds.

Figure 4 shows the time histories of the air gap variations for a vehicle operating at 400 kph. The deviations are within the safety limits. The effect of the integral action ensures that zero steady-state gap errors are achieved. Figure 5 summarizes the maglev system performance under a 100 kph cross-wind gust for different vehicle speeds. The gap variation increases with vehicle speed and the safety-related performance measure is satisfied for all speeds tested. The input voltage increases with vehicle speed and the only violation is the minimum voltage at 500 kph which exceeds the limit of −300 V slightly. The peak lateral and vertical RMS accelerations for different vehicle speeds are plotted with the minimum ISO 1 hour boundary (0.0275 *g* @ 1 ~ 2 Hz) and 1 minute boundary (0.0647 *g* @ 1 ~ 2 Hz). The results show that the maximum carbody acceleration complies with the ISO 1 minute ride quality criterion for all speeds tested. Since the cross-wind gust acts like a step disturbance at high vehicle speeds, the vehicle states return to their nominal values in a few seconds and thus the 1 minute criterion is sufficient.

The simulation results indicate that cross-wind gust has a significant impact on vehicle performance at high speed. Increasing the magnet cant angle may improve vehicle performance under strong cross-wind gust. For instance, at a vehicle speed of 500 kph, the peak voltage can be reduced from −311 V to −200 V if a 45 deg cant angle is used. However, a larger cant angle requires a larger magnetic force to balance the vehicle weight. Further sensitivity analyses on the magnet cant angle are suggested.

3.2.2 Example 2: Vehicle Traversing a Flexible, Elevated Guideway. The purpose of this example is to characterize the vehicle/guideway interaction under the influence of guideway flexibility. It is assumed that there are no guideway irregularities and preview control is not applied. Three mode shapes are used in solving the guideway deflection (where the accuracy of the solution has been verified in Wang, 1995).

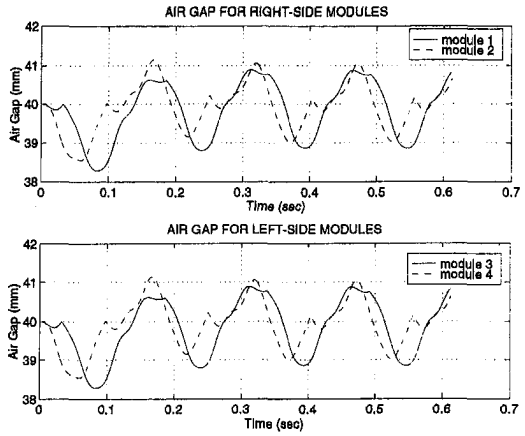

Fig. 6 Air gaps for case of flexible guideway at 500 kph vehicle speed

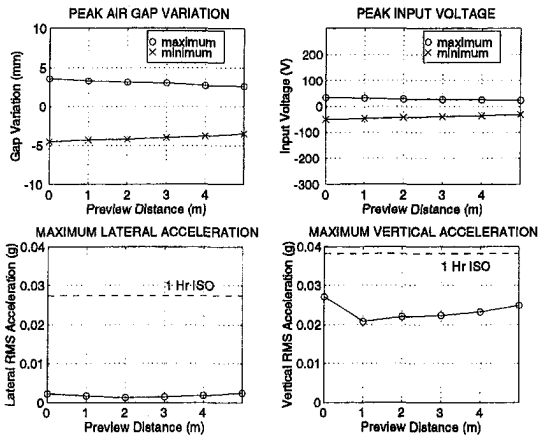

Fig. 8 Maglev system performance under combined irregularity

The vehicle operates on a 4-span flexible guideway at vehicle speeds ranging from 100 kph to 500 kph. Figure 6 shows the steady-state response of the air gap variations at 500 kph. The time histories for the right and left rails are identical in the figure, a result of the fact that the guideway flexibility on both rails is the same. Figure 7 summarizes the maglev system performance at five different vehicle speeds. The maximum gap error is 4.88 mm at 200 kph which is within the safety margin of 10 mm. The maximum peak input voltage is −51.6 V at 200 kph which is well below the ±300 V limit. Figure 7 also depicts the influences of guideway flexibility on carbody acceleration as a function of vehicle speed. The relatively high vertical acceleration around 200 kph can be interpreted in terms of the vehicle crossing frequency (vehicle speed/guideway span length) and the natural frequencies of the maglev vehicle. Under the effect of guideway flexibility, the vehicle is excited periodically with an excitation frequency equal to the vehicle crossing frequency. If the vehicle crossing frequency is close to one of the vehicle natural frequencies, the vehicle vibrations may be amplified significantly, depending on the amount of damping. At a vehicle speed of 200 kph, the vehicle crossing frequency is 2.61 Hz which is close to 2.74 Hz (17.2 rad/s), the natural frequency of the lightly damped carbody mode (see Table 3). Hence, a dynamic amplification is experienced. In this example, a higher operating speed is suggested for reducing the effect of guideway flexibility.

3.2.3 Example 3: Vehicle Performance on a Flexible Irregular Guideway. To illustrate the combined influence of guideway irregularities and deflections upon vehicle performance, the maglev vehicle was tested at 500 kph on a 4-span flexible guideway with guideway roughness and step, ramp, and camber geometry errors.

The simulation studies were performed assuming the guideway profile depicted in Fig. 3. The effect of preview control on vehicle performance was examined. The results are summarized in Fig. 8 which displays the peak values of the air gap, input voltage, and RMS accelerations for different preview distances. The results indicate that the peak input voltage and air gap variation decrease as the preview distance increases. With a 5 m preview distance, the peak voltage (−31.0 V) is 62.2% of the baseline case without preview (−49.8 V), implying a significant energy saving. For all cases tested, the maximum gap error is well below the 10 mm limit. Figure 8 also shows that the ISO 1 hour criterion is satisfied for all cases. However, the vertical peak RMS acceleration has a minimum at 1 m preview distance. As the preview distance increases further, the acceleration increases. This is caused by the fact that there is a trade-off between the gap error and carbody acceleration. Increasing preview distance tends to reduce the gap error but raises the acceleration. Thus, it can be concluded that the preview control may reduce the gap error as well as the magnet input voltage and there is a characteristic preview distance that minimizes the carbody acceleration. The worst case shown in Fig. 8 is the baseline one with zero preview distance having the highest values in voltage, gap error, and vertical RMS acceleration. Figure 9 displays the time histories of the air gap variations at a 500 kph vehicle speed. The corresponding frequency responses for the vehicle RMS accelera-

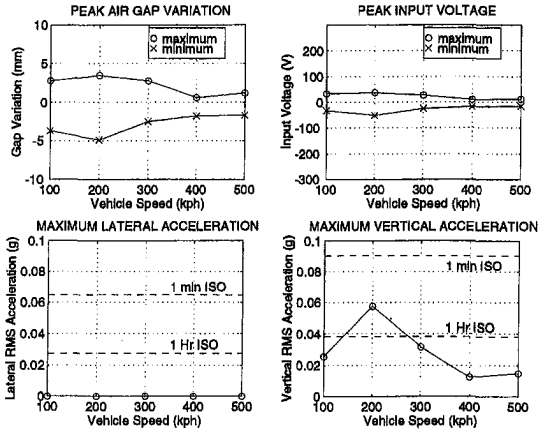

Fig. 7 Maglev system performance under guideway flexibility

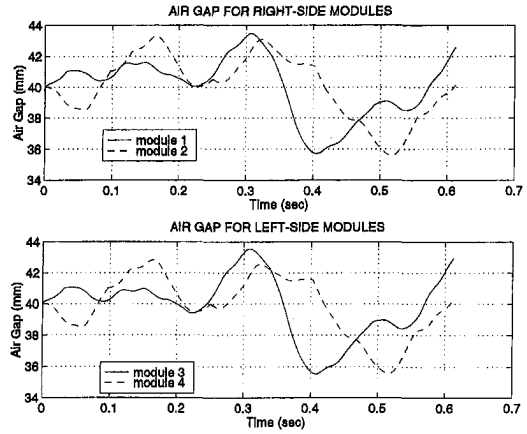

Fig. 9 Air gaps for case of combined irregularity at 500 kph

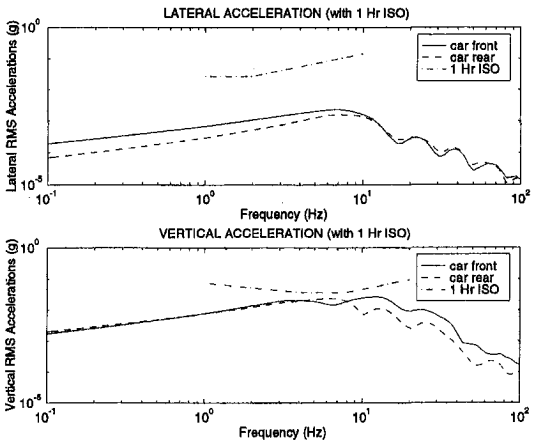

Fig. 10 RMS accelerations for case of combined irregularity at 500 kph

tions in the lateral and vertical directions are shown in Fig. 10. The results indicate that both the lateral and vertical acceleration levels are below the ISO one-hour limit.

4 Conclusion

A control law based on optimal preview control with integral action is designed for the combined lift and guidance system of an EMS maglev vehicle. The effectiveness of the control law is examined using a realistic model which includes the vehicle dynamics in the lateral, vertical, roll, pitch, and yaw directions, the magnet dynamics, and the effects of guideway flexibility and irregularity and cross-wind gust.

Simulation results reveal that preview control may reduce the input voltages substantially. Although the input voltages and gap errors decrease as the preview distance increases, the vehicle performance is limited due to a trade-off between the acceleration and gap error. It was found that there exists a characteristic preview distance that optimizes the maglev system performance.

The vehicle performance using feedback control without preview has been evaluated in the face of cross-wind gust and guideway flexibility. It was shown that cross-wind gust affects both the lateral and vertical motions due to the inclination of the magnets and produces a significant aerodynamic loading on the vehicle at high vehicle speed. Under the influence of guideway flexibility, a dynamic amplification can be experienced at a moderate vehicle speed. Identifying and shifting this critical speed away from the vehicle operating speed is an important issue in the controller design. Future studies may also explore the use of the average guideway deflection as part of the preview information to improve performance and reduce resonance.

Acknowledgment

The work described in this paper is based in part on studies performed at Carnegie Mellon Research Institute (Pittsburgh, PA) in support of the Volpe Center activities on the FRA sponsored High Speed Guided Ground Transportation (HSGGT) safety program. The authors are grateful to Mr. D. Tyrell and Dr. H. Weinstock (DOT's Volpe Center, Cambridge, MA), to Dr. I. Haque (Clemson University), and to engineers at Battelle (Columbus, OH) for their technical contributions. The authors also thank the reviewers for their thoughtful suggestions.

References

Anderson, B. D. O., and Moore, J. B., 1990, *Optimal Control: Linear Quadratic Methods,* Prentice Hall, Englewood Cliffs, NJ.

Bender, E. K., 1968, "Optimum Linear Preview Control With Application to Vehicle Suspension," ASME *Journal of Basic Engineering,* Vol. 90, No. 2, pp. 213–221.

Bryson, A. E. and Ho, Y., 1969, *Applied Optimal Control: Optimization, Estimation, and Control,* Blaisdell Publishing, Waltham, MA.

Fujioka, T., and Yamada, H., 1996, "Preview Control of Active Suspension for Railway Vehicles," *Proceedings of the ASME Dynamic Systems and Control Division,* DSC. Vol. 58, pp. 149–156.

Garg, D. P. and Barrows, T. M., 1981, "Modeling and Dynamic Response of Maglev Vehicles Subjected to Crosswind Gusts," ASME JOURNAL OF DYNAMIC SYSTEMS, MEASUREMENT, AND CONTROL, Vol. 103, pp. 251–258.

Hać, A., 1992, "Optimal Linear Preview Control of Active Vehicle Suspension," *Vehicle System Dynamics,* Vol. 21, pp. 167–195.

Heinrich, K. and Kretzschmar, R. eds., 1989, *Transrapid Maglev System,* Hestra-Verlag, Dramstadt.

ISO, 1978, "Guide for the Evaluation of Human Exposure to Whole-Body Vibration," *ISO Standard 2631,* International Organization for Standardization.

Jezequel, L., and Roberti, V., 1996, "Optimal Preview Semiactive Suspension," ASME JOURNAL OF DYNAMIC SYSTEMS, MEASUREMENT, AND CONTROL, Vol. 118, Mar., pp. 99–105.

Katz, R. M., Nene, V. D., Ravera, R. J., and Skalski, C. A., 1974, "Performance of Magnetic Suspensions for High Speed Vehicles Operating Over Flexible Guideways," ASME JOURNAL OF DYNAMIC SYSTEMS, MEASUREMENT, AND CONTROL, June, pp. 204–212.

Kortüm, W. and Utzt, A., 1984, "Control Law Design and Dynamic Evaluations for a Maglev Vehicle With a Combined Lift and Guidance Suspension System," ASME JOURNAL OF DYNAMIC SYSTEMS, MEASUREMENT, AND CONTROL, Vol. 106, pp. 286–292.

Langlois, R. G. and Anderson, R. J., 1995, "Preview Control Algorithms for the Active Suspension of an Off-Road Vehicle," *Vehicle System Dynamics,* Vol. 24, pp. 65–97.

Louam, N., Wilson, D. A., and Sharp, R. S., 1992, "Optimization and Performance Enhancement of Active Suspensions for Automobiles under Preview of the Road," *Vehicle System Dynamics,* Vol. 21, pp. 39–63.

Peng, H., and Tomizuka, M., 1993, "Preview Control for Vehicle Lateral Guidance in Highway Automation," ASME JOURNAL OF DYNAMIC SYSTEMS, MEASUREMENT, AND CONTROL, Vol. 115, pp. 679–686.

Snyder, J. E., and Wormley, D. N., 1977, "Dynamic Interactions Between Vehicles and Elevated, Flexible Randomly Irregular Guideways," ASME JOURNAL OF DYNAMIC SYSTEMS, MEASUREMENT, AND CONTROL, Mar., pp. 23–33.

Tomizuka, M., 1976, "Optimal Linear Preview Control With Application to Vehicle Suspension—Revisited," ASME JOURNAL OF DYNAMIC SYSTEMS, MEASUREMENT, AND CONTROL, Vol. 98, No. 3, pp. 309–315.

Wang, S. K., 1995, "Levitation and Guidance of a Maglev Vehicle Using Optimal Preview Control," Doctoral Dissertation, Department of Mechanical Engineering, Carnegie Mellon University, May.

Wormley, D. N., Thornton, R. D., Yu, S.-H., and Cheng, S., 1992, "Interactions Between Magnetically Levitated Vehicles and Elevated Guideway Structures," U.S. Department of Transportation Technical Report DOT/FRA/NMI-92/23.